

Supporting Information

**Drug Self-Framework Delivery System-Coated Gold Nanorods for  
Multi-Modal Imaging and Combination Therapy for Breast Cancer**

Shenglei Hou,<sup>a,b</sup> Yuan Zhang,<sup>c</sup> Meng Lian,<sup>d</sup> Xin Xie,<sup>e</sup> Qinghua Lu,<sup>f\*</sup> and Qiqing Zhang<sup>a,c,g,\*</sup>

<sup>a</sup> Institute of Biomedical Engineering, The Second Clinical Medical College, Jinan University (Shenzhen People's Hospital), Shenzhen 518020, China; Post-doctoral Scientific Research Station of Basic Medicine, Jinan University, Guangzhou 510632, P. R. China.

<sup>b</sup> The First Dongguan Affiliated Hospital, Guangdong Medical University, Dongguan 523722, P. R. China.

<sup>c</sup> Fujian Bote Biotechnology Co. Ltd., Fuzhou, Fujian 350013, P. R. China

<sup>d</sup> Shandong Engineering Laboratory for Clean Utilization of Chemical Resources, Weifang University of Science and Technology, Weifang, 262700, China

<sup>e</sup> The First Affiliated Hospital (Shenzhen People's Hospital), Southern University of Science and Technology, Shenzhen, 518055, China.

<sup>f</sup> School of Chemical Science and Engineering, Tongji University, Shanghai 200092, P. R. China.

<sup>g</sup> Institute of Biomedical Engineering, Chinese Academy of Medical Sciences and Peking Union Medical College, Tianjin 300192, P. R. China

\*Corresponding author:

Prof. Qiqing Zhang

Institute of Biomedical Engineering, the Second Clinical Medical College (Shenzhen People's Hospital) of Jinan University, Shenzhen, Guangdong 518020, P. R. China.

mail: zhangqiq@126.com

Prof. Qinghua Lu

School of Chemical Science and Engineering, Tongji University, Shanghai, P. R. China.

Email: 16115@tongji.edu.cn.

## EXPERIMENT SECTION

### Materials

Hexachlorocyclotriphosphazene (HCCP) was obtained from Tokyo Chemical Industry (Japan) Co, Ltd.  $\text{HAuCl}_4 \cdot 4\text{H}_2\text{O}$ , Cetyltrimethylammonium Bromide (CTAB),  $\text{NaBH}_4$ ,  $\text{AgNO}_3$  and L-Ascorbic acid were purchased from Sigma-Aldrich (Shanghai). Doxorubicin (DOX), HCl (37%), acetonitrile (MeCN), triethylamine (TEA), and glutathione (GSH) were purchased from Shanghai Macklin Biochemical Co. Ltd.  $(\text{H-Cys-OMe})_2 \cdot 2\text{HCl}$  was obtained from GL Biochem (Shanghai) Co. Ltd. The Annexin V-FITC/PI Cell Apoptosis Kit and LysoTracker Green were provided by Thermo Fisher Scientific (Shanghai, China). Fetal bovine serum (FBS), Dulbecco's Modified Eagle Medium with High Glucose (DMEM) was provided by Gibco (USA). Penicillin/streptomycin and the Cell Counting Kit-8 (CCK-8) were provided by Beyotime Biotechnology Co. Ltd (China). Milli-Q water (Millipore) was used in all experiments. MCF-7 cells were provided by the Shanghai Institute of Biochemistry and Cell Biology, Chinese Academy of Science. Female BALB/c nude mice (4–5 weeks old) were provided by GemPharmatech Co, Ltd.

### Characterization

The morphologies of the resultant Au NRs and Au NRs@DSFDSs NPs was analyzed by Field emission scanning electron microscopy (FE SEM, Netherlands, Philips Sirion 200, 20 kV) and Transmission electron microscopy (TEM, Japan, JEOL JEM-2100, 200 kV). Ultraviolet-visible (UV-vis) absorption spectra were recorded by the PerkinElmer Lambda 1050+ UV/VIS/NIR Spectrometer. A Paragon 1000 (PerkinElmer) spectrometer was applied to record Fourier-transform infrared (FT-IR) spectra. Photographs were collected by a digital camera (IXUS 800IS, Canon). Dynamic light scattering (DLS) measurements were recorded on a Malvern Zeta Sizer Nano ZS by using a 633 nm laser. A spectrofluorometer FS5 (Edinburgh instruments) was used to record fluorescence spectra. The fluorescence images of cells were collected by a TCS SP8 STED 3× super-resolution multiphoton confocal microscope (Leica, He-Ne and Ar lasers). The  $^{31}\text{P}$  NMR spectra were recorded on Bruker AVANCE III 400 MHz and

600 MHz (Germany) spectrometers, with chemical shifts quoted relative to  $K_2HPO_3$ . The Vevo LAZR-X ultrasonic/photoacoustic multimode imaging system (Fujifilm) were used to collect the photoacoustic imaging of MCF-7 tumor-bearing mice injecting with Au NRs@DSFDSs NPs. The photothermal imaging of MCF-7 tumor-bearing mice injecting with Au NRs@DSFDSs NPs were collected by an infrared thermal imaging system.

### **Synthesis of Au NRs@DSFDSs NPs**

The synthesis of Au-CTAB NRs. Au-CTAB NRs are synthesized according to previously reported literature.<sup>[1]</sup>

Ligand exchange of Au-CTAB NRs. Au-CTAB NRs were dispersed and volumetric with ultrapure water. 9mL Au-CTAB NRs solution was taken for reserve. 1mL CysM ( $1 \times 10^{-3}$  mM) solution was added into 9mL Au-CTAB NRs solution. The solution was rapidly stirred for 3min and left for 12h. Finally, the Au-CysM NRs were obtained by centrifuge and dispersed in acetonitrile.

The synthesis of Au NRs @DSFDSs NPs. Au NRs @DSFDSs NPs was synthesized by the following steps. Firstly, the synthesis of HCCP-CysM oligomer was proceeding according to the previously published method.<sup>[2]</sup> Au-CysM NRs acetonitrile dispersion (2mL) was fully dispersed in 40mL acetonitrile. Then, 0.4 mL HCCP-CysM oligomer and 30mg DOX was added to the above reaction solution and finally followed by 2mL triethylamine under ultrasonic irradiation. Ultrasonic irradiation (100w, 40k Hz) was conducted for 8 h at room temperature. The resulting product was collected by centrifugation (100280 rpm) for 5 minutes, and washed with 10 ml ultrapure water and ethanol for three times, respectively. Then the Au NRs@DSFDSs NPs were collected by vacuum dry at room temperature.

### ***In vitro* Drug Release**

Dialysis was used to monitor DOX-release from Au NRs@DSFDSs NPs *In vitro*. Au NRs@DSFDSs NPs (10 mg) was added into dialysis tubes (1 KD) with the dialyzate of phosphate-buffered saline solution (PBS, 100 mL, pH 7.4, 6.5 or 5.5 with or without 10  $\mu$ M GSH) under stirring at 37°C. Standard curves of UV absorbance at 480 nm of

free DOX in PBS solutions at different concentrations (Figure S3) were achieved. The dialyzates were collected at different time points and the accumulation mass of released DOX was calculated by the standard curves.

### **The photothermal conversion performance of Au NRs@DSFDSs NPs**

In order to measure the photothermal conversion performances of Au NRs@DSFDSs NPs, the varied concentrations (0, 20, 40 and 80  $\mu\text{g L}^{-1}$ ) of Au NRs@DSFDSs NPs solutions in quartz cuvettes were irradiated with a 1300 nm laser at different power densities (1.0, 1.5 and 2.0  $\text{W cm}^{-2}$ ) for 5 min. The temperatures of Au NRs@DSFDSs NPs solutions were recorded with an infrared thermal imaging system. The temperature was recorded one time per 30 s. The PT imaging and the temperature change curves during four repeated 1300 nm laser on/off cycles of the PBS solution, Au-CTAB NRs, Au-CysM NRs and Au NRs@DSFDSs NPs under the 1300 nm laser irradiation (1.5  $\text{W cm}^{-2}$ , 5 min) *in vitro* were recorded with an infrared thermal imaging system.

### ***In vitro* Uptake**

MCF-7 cells were seeded into a four-chamber glass bottom dish and incubated overnight. Cells were incubated with medium containing Au NRs@DSFDSs NPs for 2 h and then washed three times with cold PBS. The MCF-7 cells were cultured with fresh medium for a further 1, 3, 6 and 12 h. The cells were stained with DMEM supplemented with LysoTracker Green. After incubation for 1 h, the cells were washed twice with cold PBS, fixed with paraformaldehyde (4 wt%) for 30 min, and then washed twice with cold PBS. Confocal laser scanning microscopy was used to image the fixed cells.

Immunofluorescence was used to evaluate PTT efficacy of Au NRs@DSFDSs NPs on MCF-7 cells.

Cells were seeded in 6-well culture plates for overnight incubation, treated with Au NRs@DSFDSs NPs for 2 h, and then washed twice with cold PBS. No-treatment cells served as control. Cells of blank group were treated with 1300 nm laser irradiation for 5 min (1.5  $\text{W cm}^{-2}$ ). Cells of Au NRs@DSFDSs were treated with 1300

nm laser irradiation for 10min ( $1.5 \text{ W cm}^{-2}$ ) or not. The cells of each group were cultured for another 6 hours. Finally, the staining was carried out according to the CFDA-SE staining kit. Fluorescence images of the MCF-7 cells were collected by fluorescence microscope.

### **Cell Viability Test**

MCF-7 cells ( $5 \times 10^4$  cells  $\text{mL}^{-1}$ , 200  $\mu\text{L}$  of medium) were seeded into a 96-well culture plate. After overnight incubation, different concentrations of free DOX, Au NRs, DOX-CysM-CPPZ NPs or Au NRs@DOX-CysM-CPPZ NPs in culture medium without FBS were co-incubated with cells for 4 h. After incubation, the cells were washed twice with cold PBS, and added with fresh medium. The cells were incubated with fresh media for a further 24 h and then each well was treated with WST-8 reagent (10  $\mu\text{L}$ ). The cells of Au NRs or Au NRs@ DOX-CysM-CPPZ NPs groups were exposed to 1300 nm laser with  $1.5 \text{ W cm}^{-2}$  for 10min. Then the cells were cultured for further 24, 48 or 72 hours. Finally, 20 $\mu\text{L}$  CCK-8 reagent was added to each hole for further 1 hour incubation. The absorbance at 450 nm was record on amicroplate reader (Bio-Rad, model 680). Cell viability was calculated as the percentage absorbance of the sample well compared to that of the controls.

The cytotoxicity of each treatment was also evaluated by quantitative analysis of MCF-7 cell apoptosis. MCF-7 cells ( $5 \times 10^4$  cells per well) were seeded into a 24-well plate. The cells were treated with PBS, free DOX, Au NR, DOX-CysM-CPPZ NPs or Au NRs@ DOX-CysM-CPPZ NPs (at an equivalent drug concentration of 2  $\mu\text{M}$ ) and incubated for 2 days. Flow cytometry was used to measure and quantify apoptosis using an Annexin V-FITC/PI Apoptosis Detection Kit.

### **Multi-modal Imaging *In Vivo***

Female BALB/c nude mice (4–5weeks old) were provided by GemPharmatech Co, Ltd. All animal experiments were conducted in strict observance of the guide for the care and use of laboratory animals by Shenzhen People's Hospital Animal Study Committee. MCF-7 cells ( $10^7$ ) were implanted into the flank region of the mice by subcutaneous injection.

### *FL imaging in vivo and biodistribution*

When the tumor was about 300–400 mm<sup>3</sup>, The tumor-bearing mice were randomly divided into three groups of five. The mice were injected with PBS (120 µL), free DOX, DOX-CysM-CPPZ NPs, or Au NRs@DSFDSs NPs via the tail vein, at an equivalent DOX concentration of 0.17 mg mL<sup>-1</sup>. After injection, the *in vivo* red fluorescence signal of free DOX at different time points was recorded using an *ex/in vivo* imaging system with a 488/590 nm filter setting. The mice were sacrificed 24 h after injection and the key organs and tumors were excised for imaging and biodistribution analysis. The DOX fluorescence signal was obtained using the 488/590 nm filter setting.

### *Photothermal Imaging in vivo*

The tumor-bearing mice were intravenously injected with PBS or Au NRs@DSFDSs NRs (38.4 mg Au/kg body weight). After injection for 24 h, a 1300 nm laser at 1.5 W cm<sup>-2</sup> was used to irradiate the tumor regions of the mice. The temperature elevations of the tumor site were recorded at different time points (1, 2, 3, 4, and 5 min), and imaged with an infrared thermal imaging system.

### *PA Imaging in vitro and in vivo*

Different concentrations of Au NRs@DSFDSs NRs (0, 10, 20, 40, and 80 µg/mL) were placed in the thin pipe, which was placed in phantoms. The Vevo LAZR-X ultrasonic/photoacoustic multimode imaging system (Fuji) was used to record the PA images at different concentrations 1300 nm wavelength.

When the tumor volumes reached about 300–400 mm<sup>3</sup>, the PA imaging of the mice was performed. Briefly, the MCF-7 tumor-bearing mice were intravenously injected with Au-CysM NRs or Au NRs@DSFDSs NRs (38.4 mg of Au/kg body weight). The Vevo LAZR-X ultrasonic/photoacoustic multimode imaging system (Fuji) was used to record the PA images of 1300 nm wavelength at different time points (0, 2, 6, 12 and 24 h).

### **Tumor Inhibition Efficacy and Evaluation of Biosafety *in vivo***

When tumor volumes reached about 100 mm<sup>3</sup>, the tumor-bearing mice were divided into five groups with five mice in each group randomly : (1) PBS, (2) free DOX, (3) Au-CysM NRs + laser, (4) Au NRs@DSFDSs NRs, (5) Au NRs@DSFDSs NRs+ laser. The dose of the DOX and Au NRs were 3 and 28.4 mg/kg body weight, respectively. The 5 min laser treatments were carried out by a 1.5 W cm<sup>-2</sup> power of 1300 nm laser. The tumor volume was measured at every other day during the 16-day therapy course. The volumes of tumor in each group were worked out according to (length × width)<sup>2</sup> /2. The relative tumor volume was determined as V/V<sub>0</sub> (V<sub>0</sub> refers to the tumor volume at day 0). Upon termination of the regimen, all of the mice were humanely sacrificed, and the tumors were harvested, fixed and embedded for tumor biopsies of TUNEL assay. The tumor inhibition ratio (TIR) was calculated as:  $TIR = ((M_{\text{tumor weight of mice in PBS group}}) - (M_{\text{tumor weight of mice in each different group}})) / (M_{\text{tumor weight of mice in each different group}}) \times 100\%$ .

The body weights at every other day during the 16-day therapy course and the hematoxylin and eosin (H&E) staining of key organs including lung, liver, spleen, kidney, and heart was performed to evaluate the toxicity and side effects of different formulas in vivo.

## FIGURE AND CAPTION SECTION

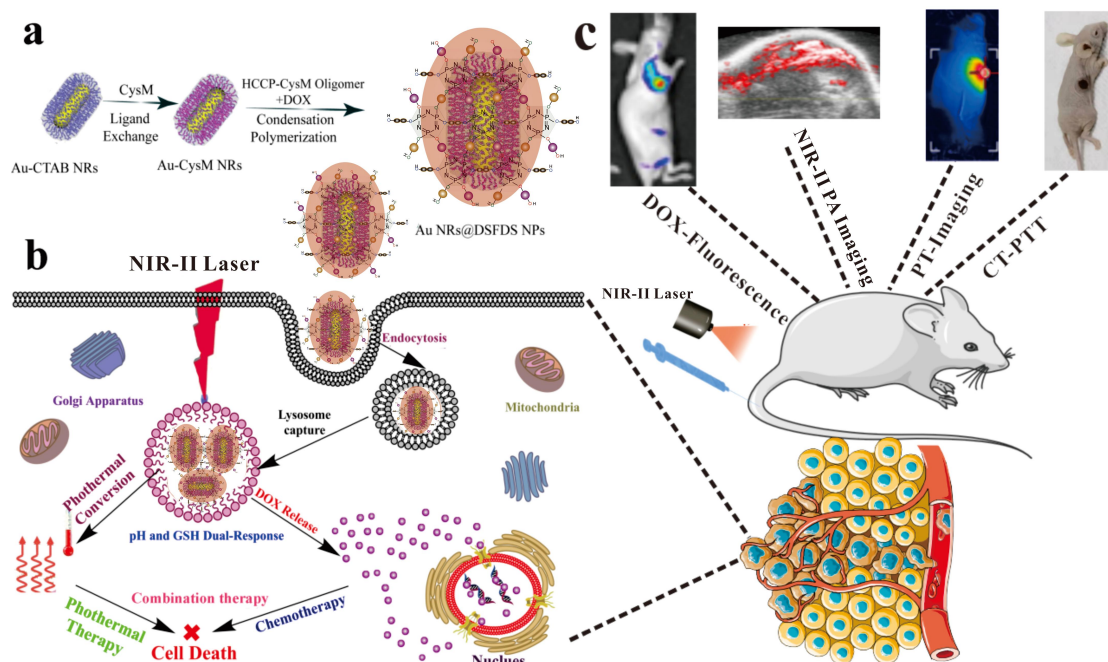


**Fig. S1** (a) synthesis of Au NRs@DSFDSs NPs for synergistic chemo-PT therapy against cancer cells with DSFDS polymer layer Au NRs. (b) cell internalization of Au NRs@DSFDSs NPs, DOX release induced by low pH and high GSH in cancer cells and synergistic chemo-PT therapy to kill cancer cells. (c) illustration of one conjugate nanoparticle of Au NRs@DSFDSs NPs for multi-modal PA/FL/PT imaging guided the synergistic CT-PTT in vivo.

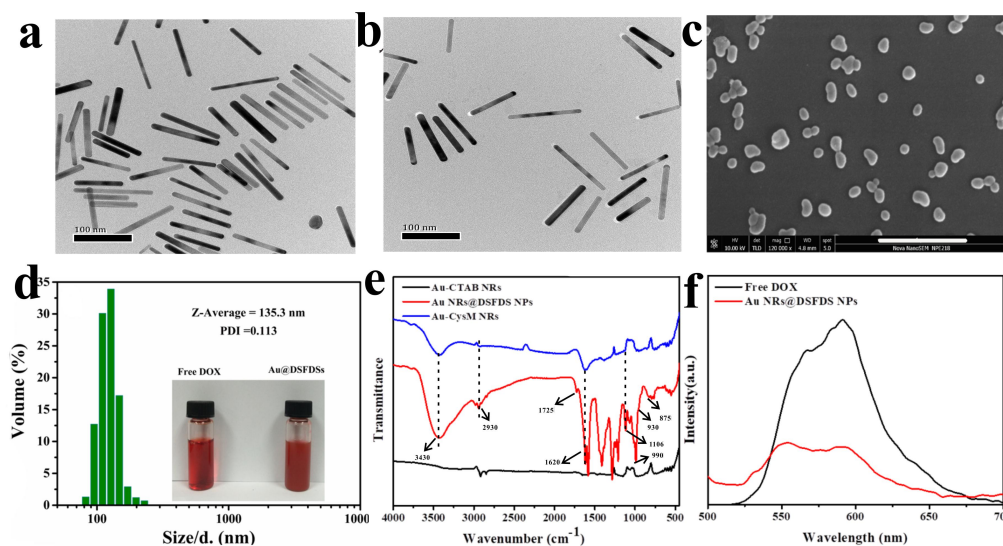


**Fig. S2** TEM of (a) Au-CTAB NRs and (a) Au-CysM NRs. (c) SEM of Au NRs@DSFDS NPs. (d) DLS data (inset: optical photography of free DOX and Au NRs@DSFDSs NPs suspensions) of Au NRs@DSFDSs NPs. (e) FTIR spectra of Au-CTAB NRs, Au-CysM NRs and Au NRs@DSFDS NPs. (f) Fluorescence spectra of free DOX and Au NRs@DSFDS NPs. Scar bars are (a) 100nm, (b) 100nm and (c) 2  $\mu$ m.

TEM images revealed that Au NRs-CTAB prepared by seed method had a uniform shape with the size of about 115 ( $\pm$ 5)  $\times$  13 ( $\pm$ 1.1) nm (Figure S2a). In order to

enhance the dispersion of Au NRs in acetonitrile, the CTAB on the surface of Au NRs can be replaced by CysM with a stronger binding capacity. After ligand exchange, the morphology of Au NRs-CysM had no change or obvious aggregation (Fig. S2b). Because the chain grows step by step during condensation polymerization, SEM and TEM images showed that Au NRs@DSFDSs NPs were uniform solid spheres with a smooth surface (Fig. 1a, S2c). As shown in dynamic light scattering (DLS) spectroscopy, the hydration diameter of Au NRs@DSFDSs NPs had a narrow unimodal distribution (Fig. S2c).

Solid-state  $^{31}\text{P}$  NMR of Au NRs@DSFDSs NPs was analyzed to prove the finished synthesis. A single peak at 21.34 ppm for was assigned to  $-\text{P}(\text{Cl})_2$  in pure HCCP (Figure 1b). After the synthesis of further Au NRs@DSFDSs NPs, the  $^{31}\text{P}$  solid-state NMR spectrum of Au NRs@DSFDSs NPs became a typical dispersion peak due to the formation of nanoparticles and the peak at 21.34 ppm assigned to  $-\text{P}(\text{Cl})_2$  became very small. Two new wide peaks at 7.54 and  $-3.08$  ppm appeared and could be assigned to  $(\text{CysM-N})-\text{P}-(\text{O-DOX})$  and  $-\text{P}-(\text{O-DOX})_2$ , respectively.

The chemical composition was checked by FT-IR (Figure S2e). The Au NRs@DSFDS NPs showed characteristic peaks of carbonyl and amino-ester groups at  $1745\text{ cm}^{-1}$  and  $1523\text{ cm}^{-1}$ . The peak at  $871\text{ cm}^{-1}$ , corresponding to the P-N of HCCP. The peak at  $1106\text{ cm}^{-1}$  was assigned to the stretching vibration of  $-\text{C}-\text{O}-\text{C}-$  in DOX. The spectrum of Au NRs@DSFDS NPs showed a new peak at  $930\text{ cm}^{-1}$ , corresponding to the stretching vibration of the  $-\text{P}-\text{N}-\text{C}-$  bond, which corroborated the formation of covalent bonding between HCCP and CysM. Furthermore, the appearance of a  $\text{P}-\text{O}-\text{Ar}$  peak at  $990\text{ cm}^{-1}$  together with the signal of phenolic hydroxyl at  $3430\text{ cm}^{-1}$ , also provided significant evidence for covalent bonding between DOX and HCCP.

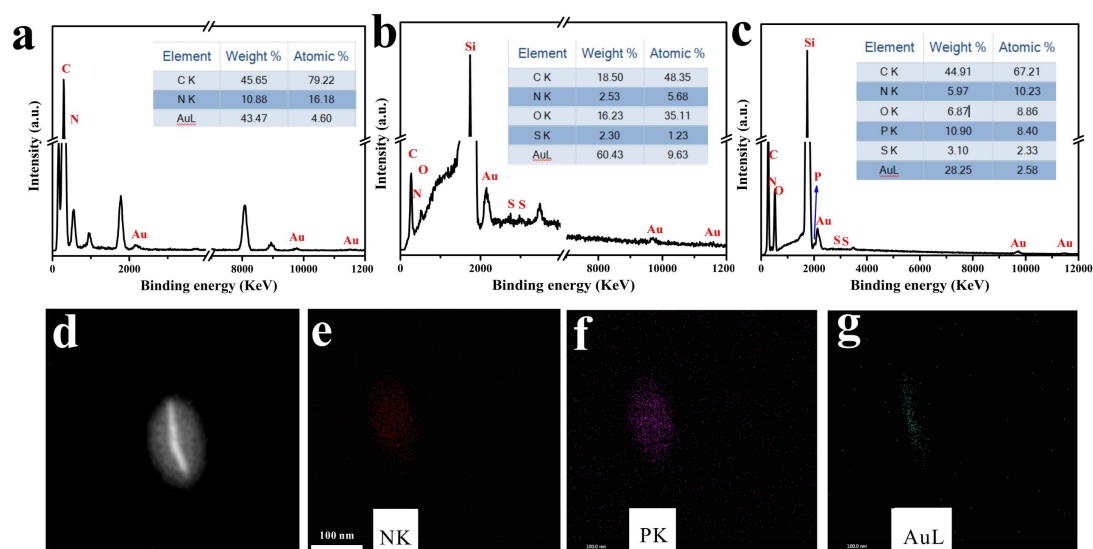


**Fig. S3** The EDS of (a) Au NRs-CTAB, (b) Au NRs-CysM and (c) Au NRs@DSFDSs NPs. (d-g) The TEM Element Mapping of Au NRs@DSFDSs NPs.

The EDX elemental analysis of Au NRs-CTAB, Au NRs-CysM and Au NRs@DSFDSs NPs (Fig.S3a-c) verifies that the surface stabilizer of Au NRs have changed from CTAB

to CysM via ligand exchange, and then the DSFDSs polymer were coated onto the surface of Au NRs by a simple condensation polymerization. Meanwhile, the elemental mapping of Au NRs@DSFDSs NPs (Fig. S3d-g) provides that the oval shell structure is indeed made of DSFDSs polymer and the rod-like core structure are actually AuNRs. All of these results indicated that the Au NRs@DSFDSs NPs was synthesized successfully.

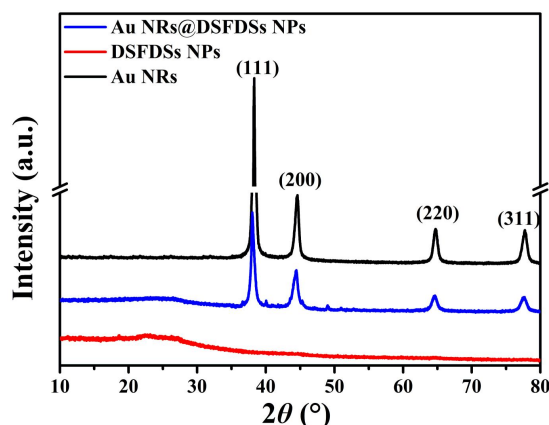


**Fig. S4** XRD patterns of Au NRs, DSFDSs NPs and Au NRs@DSFDSs NPs.

The XPS patterns of the Au NRs-CysM, DSFDSs NPs and Au NRs@DSFDSs NPs were showed in Fig. S4. The XPS patterns of the Au NRs-CysM showed the presence of Aurum with some amount of carbon, nitrogen, sulphur and oxygen, which was a result of CTAB and CysM served as surfactant. The XPS patterns of the DSFDSs NPs showed the presence of carbon, nitrogen, sulphur, phosphorus and oxygen, which was a result of HCCP, DOX and CysM served as molecule of reaction. The XPS patterns of the Au NRs@DSFDSs NPs showed the presence of Aurum, nitrogen, sulphur, phosphorus and oxygen provided by Au NRs-CysM and DSFDSs NPs, indicating that the Au NRs were coated with DSFDSs to form Au NRs@DSFDSs NPs successfully.

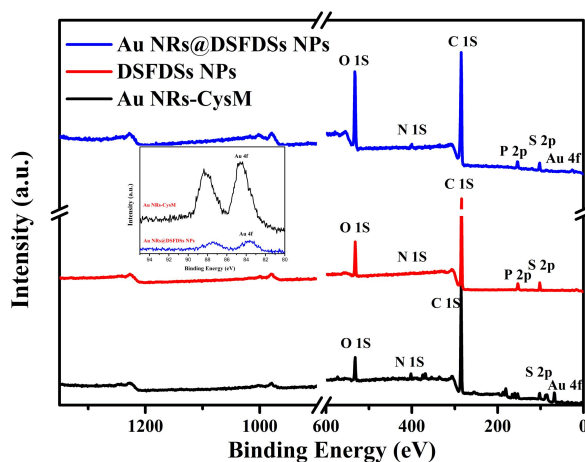


**Fig. S5** XPS patterns of Au NRs, DSFDSs NPs and Au NRs@DSFDSs NPs.

The XPS patterns of the Au NRs-CysM, DSFDSs NPs and Au NRs@DSFDSs NPs were

showed in Fig. S5. The XPS patterns of the Au NRs-CysM showed the presence of Aurum with some amount of carbon, nitrogen, sulphur and oxygen, which was a result of CTAB and CysM served as surfactant. The XPS patterns of the DSFDSs NPs showed the presence of carbon, nitrogen, sulphur, phosphorus and oxygen, which was a result of HCCP, DOX and CysM served as molecule of reaction. The XPS patterns of the Au NRs@DSFDSs NPs showed the presence of Aurum, nitrogen, sulphur, phosphorus and oxygen provided by Au NRs-CysM and DSFDSs NPs, indicating that the Au NRs were coated with DSFDSs to form Au NRs@DSFDSs NPs successfully.

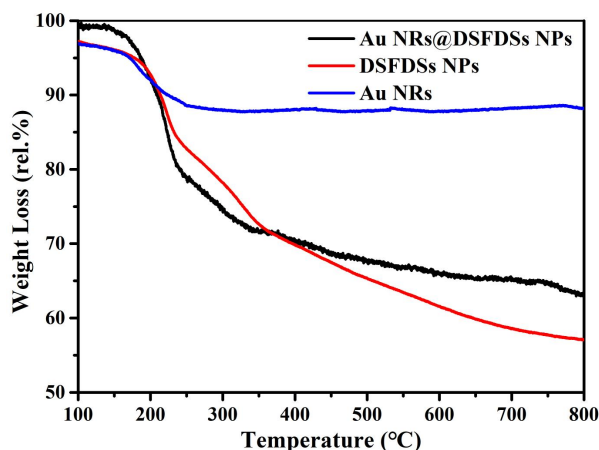


**Fig. S6** TGA patterns of Au NRs, DSFDSs NPs and Au NRs@DSFDSs NPs.

The TGA patterns of the Au NRs, DSFDSs NPs and Au NRs@DSFDSs NPs were displayed in Fig. S6. The TGA patterns of the standing Au NRs showed that the thermal decomposition of Au NRs begins at 210°C and the mass loss is about 9% at 800°C, which is the mass of the surface stabilizer of Au NRs. The TGA patterns of the DSFDSs NPs and Au NRs@DSFDSs NPs showed that the mass loss is about 2% at 100°C, which is the mass of the residual H<sub>2</sub>O in the sample. The TGA patterns of the DSFDSs NPs showed that the thermal decomposition of DSFDSs NPs begins at 200°C and the rate of residue mass is about 55%, indicating that the DSFDSs NPs exhibit an excellent thermal stability due to a highly cross-linked structure. The TGA patterns of the Au NRs@DSFDSs NPs showed that the thermal decomposition of Au NRs@DSFDSs begins at 220°C and the rate of residue mass is about 63%, which is higher than that of Au NRs@DSFDSs NPs due to the participation of Au NRs. To sum up, the Au NRs@DSFDSs NPs was synthesized successfully.

Solid-state <sup>31</sup>P NMRs, fourier transform infrared spectra (FTIR), TEM element mapping, energy dispersive spectra (EDS), X-ray diffraction spectra (XRD), thermogravimetric analysis (TGA), UV-Vis and FL spectra of Au NRs@DSFDSs NP were analyzed to prove the finished synthesis (shown in Fig. 1b, Fig. S2c, S2d, S3-S8 and S9a, b).

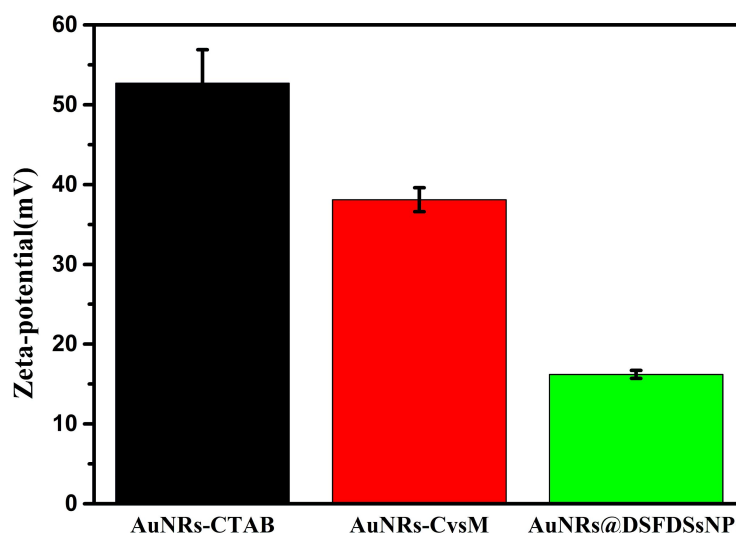


**Fig. S7** The Zeta potential of Au NRs-CTAB, Au NRs-CysM and Au NRs@DSFDSs NPs.

The zeta potential of Au NRs-CTAB, Au NRs-CysM and Au NRs@DSFDSs NPs were +52.6mV, +38.2mV and +16.2mV, indicating that the synthesis of the Au NRs@DSFDSs was successful via ligand exchange and condensation polymerization.

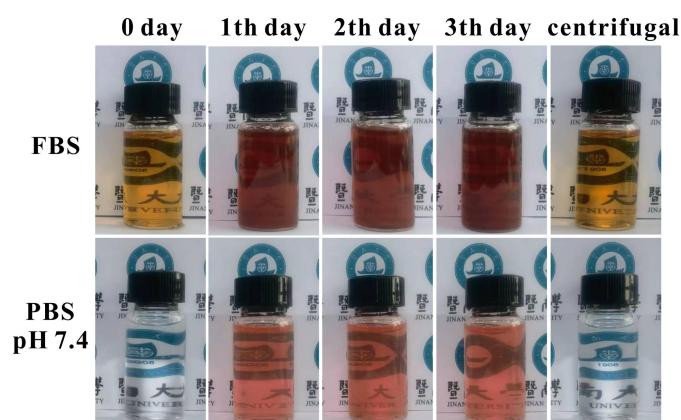


**Fig. S8** Photographs of Au NRs@DSFDSs NPs dispersed in FBS and PBS (pH 7.4) after different times or centrifugation.

Meanwhile, the Au NRs@DSFDSs NPs could be dispersed in PBS at pH 7.4 and FBS without any aggregation during 3 days (Figure S8), which may lengthen the blood circulation time *in vivo*.

The optical photography and Zeta potential was proved that Au NRs@DSFDSs NPs have the good dispersion stability in PBS and FBS (Fig. S7 and S8 b), indicating good stability of Au NRs@DSFDSs NPs under normal physiological environment.

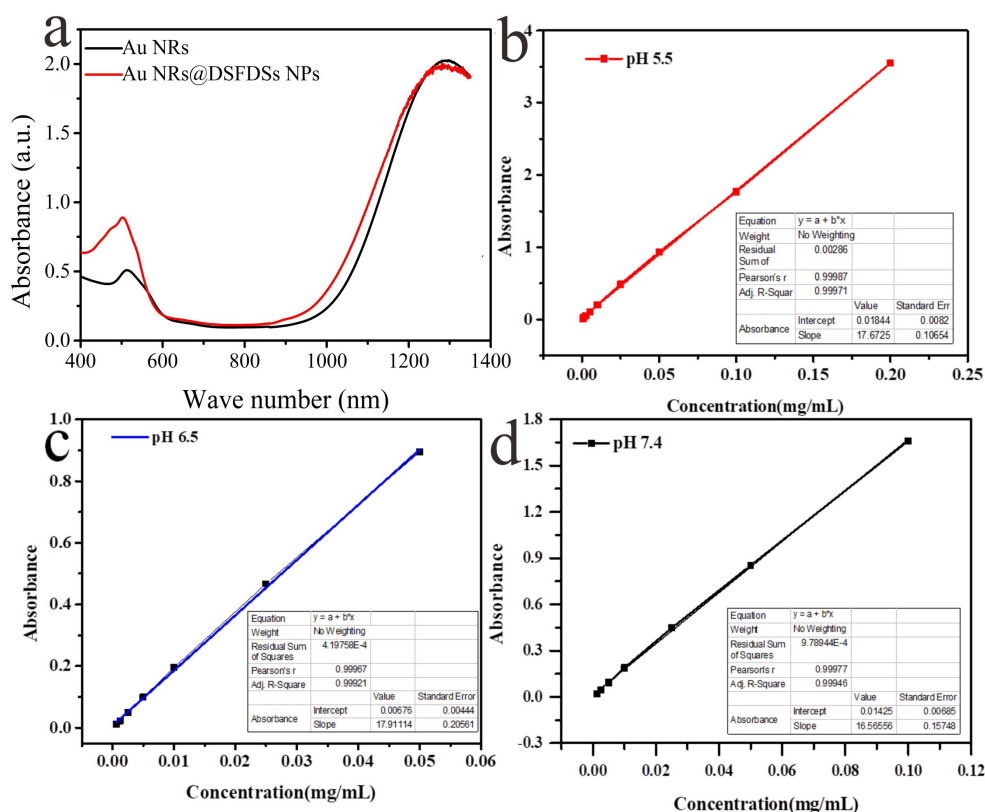


**Fig. S9** (a) UV-vis spectra of Au NRs and Au NRs@DSFDS NPs. (d) Fluorescence spectra of free DOX and Au NRs@DSFDS NPs. Standard curves of UV absorbance of DOX at 480 nm versus concentration at pH (b) 5.5, (c) 6.5 or (d) 7.4.

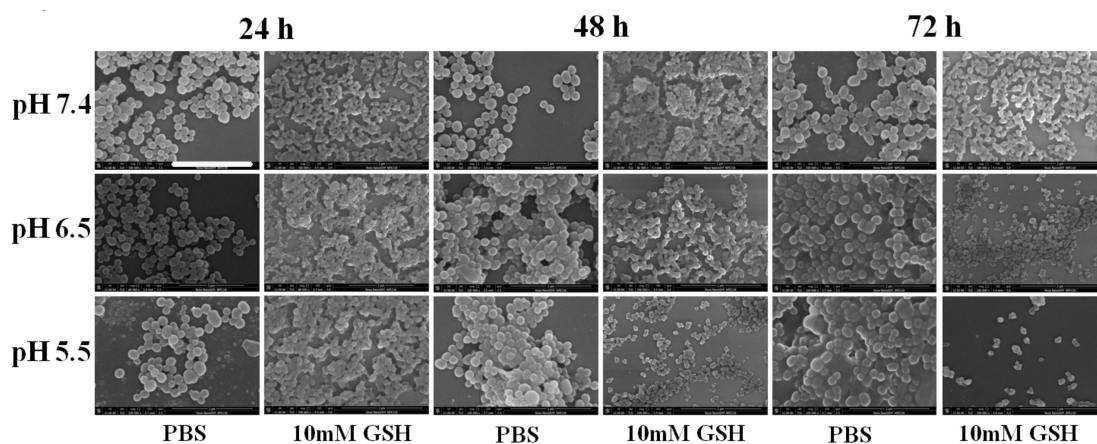


**Fig. S10** SEM images of Au NRs@DOX-CysM-CPPZ NPs showing degradation under different conditions. Scar bars are (a) 100nm, (b) 100nm and (e) 2  $\mu$ m.

The *in vitro* release behavior of Au NRs@DSFDSs NPs was evaluated by dialysis in different pH PBS with GSH or not at 37°C (as shown in Figure 1c and d). The DOX served as the framework of the cross-linked DOX-CysM-CPPZ polymer which was used as the layer of Au NRs. After the hydrolysis of phosphazene rings and fracture of

the disulfide bond of CysM under lower pH and higher GSH condition, the DOX was released. Therefore, Au NRs@DSFDSs NPs served as an ideal drug delivery system was not only stable in the blood circulation, but also rapidly releases drugs as needed when they reach the target tumor site.

However, the release rate of DOX was only 6.8% in pH 7.4 PBS without GSH after 72 h (Fig. 1c and d). As shown in the SEM images of Fig. S10, the Au NRs@DSFDSs NPs remained intact with clear boundaries, indicating the stability of Au NRs@DSFDSs NPs in blood circulation. When the pH value of PBS was adjusted to 6.5 (simulation of tumor sites) or 5.5 (simulation of lysosome), the accumulated release rates of DOX increased to 26.5% and 37.6%, respectively. DLS data and SEM images of Au NRs@DSFDSs NPs demonstrated that the nanoparticles began to degrade under the relevant conditions (as shown in Fig. S10 and S11). After adding 10 mM GSH into PBS, the accumulation release rate of DOX increased to 55% at pH 7.4 and 78% at pH 5.5 after 24h. It could even reach up to 95% in pH 5.5 PBS with 10mM GSH after 3 days. As shown in SEM images and DLS data, Au NRs@DSFDSs NPs had degraded into smaller nanoparticles and the average size reduced from 135.8 at pH 7.4 and to 76.2 nm at pH 5.5 with 10 mM GSH after incubation with PBS for 3 days. Therefore, the concentration of GSH have great effect on the release rate of DOX. Compared with the TME, there was hardly any DOX release from Au NRs@DSFDSs NPs in blood circulation.

By simulating the tissue microenvironment, multi-stage stimulation drug-release was performed to evaluate the possibility of drug-release on demand (shown in Figure 1d). As shown in multi-stage-responsive release behavior curve of DOX, the DOX-release was minimal (about 5%) in pH 7.4 PBS (simulating blood) and almost reach the platform during 4 h. Following adjusting the pH to 6.5 (simulating the extracellular microenvironment at the tumor site), the DOX-release greatly increased. Further the DOX release was enhanced upon addition of 10 mM GSH (simulating the intracellular microenvironment of tumor cells). Finally, the DOX-release was obviously increased after adjusting the pH value to 5.5 (simulating the lysosomal microenvironment). Those results demonstrated that the Au NRs@DSFDSs NPs were responsive to high level of GSH and low pH, due to the S–S bond and P–N– or P–O– bonds in the DSFDS polymer. The Au NRs@DSFDSs NPs could not only stop early drug-release in blood circulation, but also release DOX on demand after arriving at tumor sites. The TME-responsive DOX release of Au NRs@DSFDSs NPs is crucial for chemotherapy against cancer.

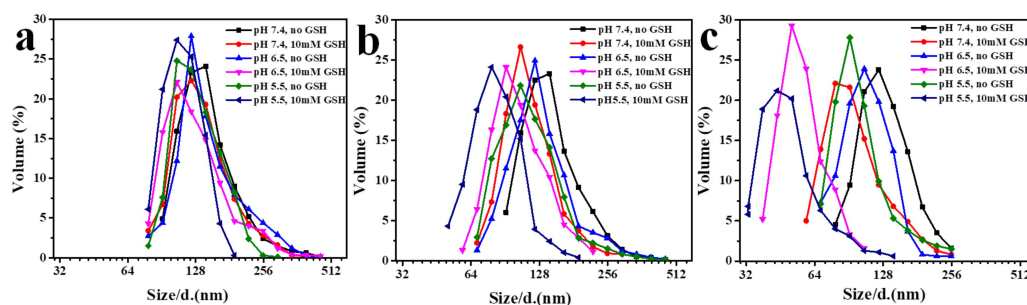


**Fig. S11** DLS data of Au NRs@DSFDS NPs during degradation in PBS at pH 7.4, 6.5 and 5.5 with or without 10 mM GSH after (a) 1 day, (b) 2 days, or (c) 3 days.

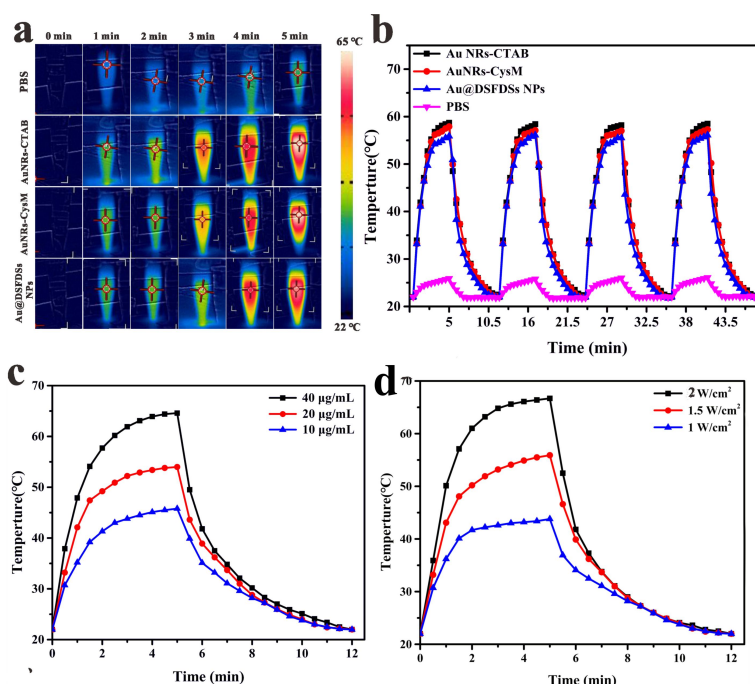


**Fig. S12** (a) The PT imaging of different formulations under the laser irradiation ( $1.5 \text{ W}\cdot\text{cm}^{-2}$ , 1300 nm, 5 min) *in vitro*. (b) The temperature change curves of different nanoparticles solution during four repeated 1300 nm laser on/off cycles. The temperature change curves of (c) different concentrations of Au NRs@DSFDSs NPs solution under the 1300 nm laser irradiation ( $1.5 \text{ W}\cdot\text{cm}^{-2}$ , 5 min) and (d)  $20 \text{ mg}\cdot\text{mL}^{-1}$  Au NRs@DSFDSs NPs solution under the 1300 nm laser irradiation for 5 min with different power during laser on/off cycles.

As shown in Fig. S12a and 12b, under 1300 nm laser irradiation with  $1.5 \text{ W}\cdot\text{cm}^{-2}$  for 5 min, the temperature of DI water with Au NRs-CTAB, Au NRs-CysM and Au NRs@DSFDSs NPs increased from  $22 \text{ }^\circ\text{C}$  to  $26$ ,  $58.7$ ,  $57.9$  and  $56.9 \text{ }^\circ\text{C}$  with a temperature difference of  $4.0$ ,  $36.7$ ,  $35.9$  and  $34.9 \text{ }^\circ\text{C}$ , respectively. Those indicated that Au NRs@DSFDSs NPs could be applied to PTT against tumor. The temperature difference increased by Au NRs-CTAB > Au NRs-CysM > Au NRs@DSFDSs NPs, which was due to the slight agglomeration of Au NRs at the time of ligand exchange. The lowest temperature difference of Au NRs @DSFDSs NPs was due to the fact that Au

NRs was coated by the polymer layer of DOX-CysM-CPPZ, which slightly reduced its photothermal conversion capacity.

As showed in Fig. S12b, the temperature heating and cooling cycle curves of Au NRs@DSFDSs NPs were basically the same with no obvious decrease, which proved that Au NRs@DSFDSs NPs had good photothermal stability. As is known to all, the temperature variation of nanoparticles with photothermal conversion ability was strongly dependent on their concentration and the energy density of near-infrared laser. As shown in Fig. S12c and S12d, the temperature variation of nanoparticles solution became higher and higher with the increasing of the concentration of nanoparticles and the energy density of the near-infrared laser. This further indicates that the increasing temperature of Au NRs@DSFDSs NPs solution is mainly induced by NIR-II laser absorption of Au NRs.

Photothermal conversion properties of Au NRs@DSFDSs NPs were determined according to the previous reports.<sup>[3, 4]</sup> Photothermal transduction efficiency ( $\eta$ ), which depends on the shape and size of Au NRs, could be regarded as the inherent property of Au NRs.  $\eta$ , which could be considered as the absorption/extinction ratio, was employed to evaluate the efficiency of the nanoparticles to convert light into heat. As shown in Fig. S12c and Fig. S12d, there were the heating profiles of Au NRs@DSFDSs NPs solution, varying the concentrations of Au NRs solution (absorbance) and power intensities of laser irradiation. The temperature rose quickly at the beginning five minutes of irradiation until attaining a plateau temperature and followed a negligible increment under 1300 nm laser irradiation (Fig. S12c and Fig. S12d). The  $\eta$  of Au-CTAB NRs, Au-CysM NRs and Au NRs@DSFDSs NPs under 1300 nm laser irradiation was calculated to be 54.3%, 52.2% and 50.3%, respectively. The  $\eta$  value of Au NRs@DSFDSs NPs was smallest, which was attributed to that the attachment of polymeric layers onto the surface of the Au NRs diminished the efficacy of the photothermal conversion by the enhancing of the scattered light. The decrease of  $\eta$  value which was induced by the DOX-CysM-CPPZ polymer layer of the Au NRs was not too much. The Au NRs@DSFDSs NPs were excellent enough to be used as a platform for the PTT against tumor.

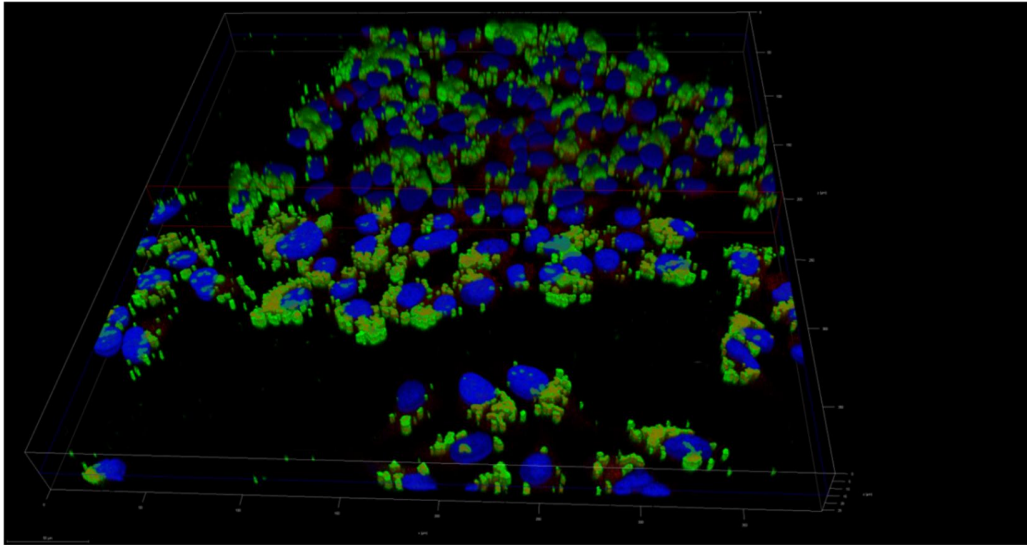


**Fig. S13.** 3D Laser confocal microscopy images of MCF-7 cells after incubation with Au NRs@DOX-CysM-CPPZ NPs for 6h (red, DOX; green, LysoTracker Green).

3D Laser confocal microscopy images and TEM of MCF-7 cells were applied to research the cell distribution of Au NRs@DSFDSs NPs and the progress of entering cells. As shown in 3D FL image of MCF-7 cell (Figure S13), the location of LysoTracker Green in lysosomes overlapped with that of Au NRs@DSFDSs NPs with the red fluorescence signal, indicating that the Au NRs@DSFDSs NPs accumulated within lysosomes. As shown in Figure 2a, TEM images of MCF-7 cells showed that the Au NRs@DSFDSs NPs could enter into cancer cell via endocytosis. Then the Au NRs@DSFDSs NPs could be accumulated within lysosomes. The Au NRs@DSFDSs NPs degraded into smaller nanoparticles and simultaneously the DOX was released, which was induced by TME. It was the first time that the intracellular degradation process of polyphosphazene nanoparticles-based DSFDS was observed.

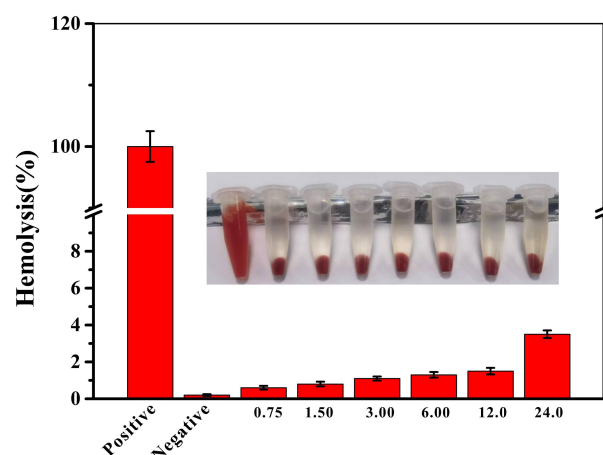


**Fig. S14** Hemolysis tests of various concentration of Au NRs@DSFDSs NPs. The insert figure was the corresponding hemolysis graph.

Hemolysis experiment show that a higher dose of Au NRs@DSFDSs NPs did not cause obvious hemolysis, indicating acceptable biocompatibility.

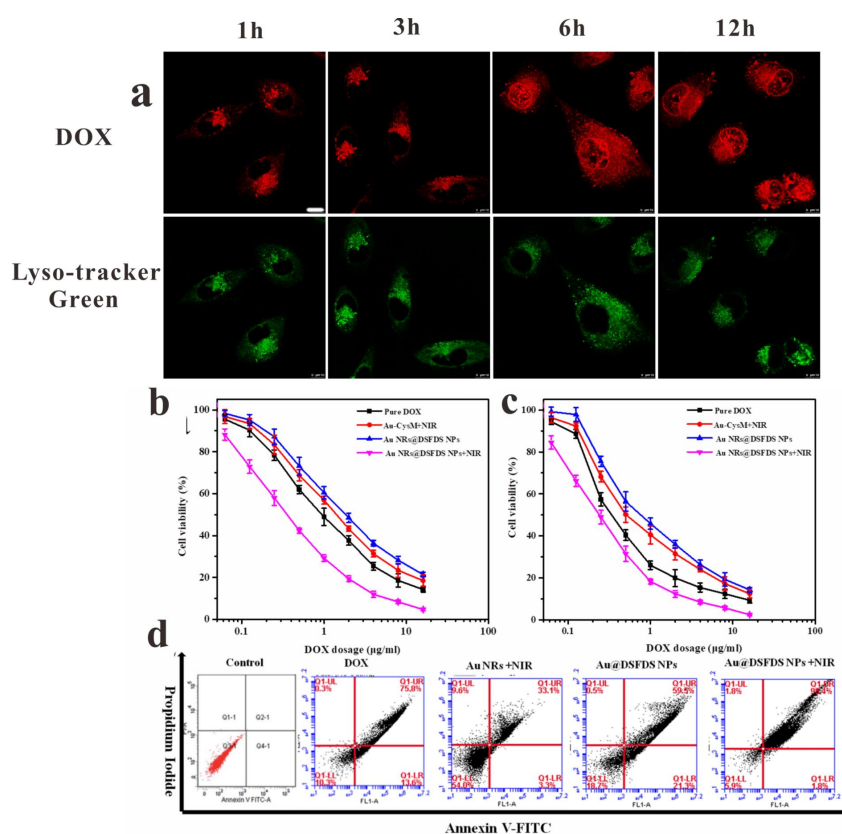


**Fig. S15** (a) Laser confocal microscopy images of MCF-7 cells after incubation with Au NRs@DOX-CysM-CPPZ NPs for different periods (red, DOX; green, LysoTracker Green). Scale bars represent 10 µm. Killing efficiencies towards MCF-7 cells when incubated with different concentrations of free DOX, Au NRs+1300 nm laser, Au NRs @DSFDS NPs or Au NRs @DSFDS NPs+1300 nm laser for (b) 24 and (c) 48h, respectively. (d) Flow cytometry analysis of MCF-7 cells cultured with different treatments for 48 h, wherein each system contained 2 mg mL<sup>-1</sup> DOX.

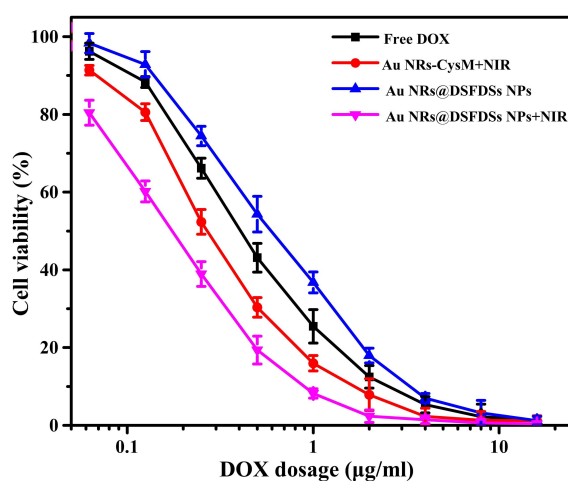


**Fig. S16** Killing efficiencies towards MCF-7 cells when incubated with different concentrations of free DOX, Au NRs+1300nm laser, Au NRs@DSFDS NPs or Au NRs@DSFDS NPs+1300nm laser for 72h.

As shown in Fig. 2c and S15a (ESI), LSCM imaging indicated that Au NRs@DSFDSs NPs could enter into the MCF-7 cells efficiently. After incubating with Au NRs@DSFDSs NPs for 1 h, there was a bright red fluorescence in the cells (shown in Fig. 2c and S15a, ESI), indicating that Au NRs@DSFDSs NPs entered into the MCF-7 cells efficiently. With the incubation time going on, the intracellular fluorescence intensity became stronger. As shown in Fig. S15a, the red fluorescence signal of Au NRs@DSFDSs NPs co-localized with lysosomes stained by LysoTracker Green, indicating transporting Au NRs@DSFDSs NPs to lysosomal compartments after cell uptake. Then, the Au NRs@DSFDSs NPs were degraded due to the trigger induced by the low pH and high GSH level in MCF-7 cells. While adding incubation time up to 6 h, the red fluorescence began to appear in the nuclei. When the DOX was released from the Au NRs@DSFDSs NPs, the free DOX could move from lysosomes to the nucleus due to net unidirectional diffusion. With the gradual nuclear accumulation of DOX, the amount of lysosomal DOX decreased over time. The Au NRs@DSFDSs NPs could be an effective chemotherapeutic because of this property. Therefore, the Au NRs@DSFDSs NPs could be used to monitor and suppress the tumor growth. Furthermore, this approach could be used to devise and track the Au NRs@DSFDSs NPs.

Immunofluorescence assay was used to evaluate the photothermal performance of Au NRs@DSFDSs NPs on MCF-7 cells. As shown in Fig. 2b, the MCF-7 cells of the control group and that of the 1300 nm laser group had good cell shape without necrosis. Compared with the control group, the number of Au NRs@DSFDSs NPs-treated MCF-7 cells decreased significantly, which is due to the chemotherapy of Au NRs@DSFDSs NPs. After the MCF-7 cells was treated Au NRs@DSFDSs NPs and irradiated by 1300 nm laser, almost all the cells died within the irradiation range, which was attributed to the synergistic killing effect of Au NRs@DSFDSs NPs on cancer cells via synergistic CPTT. While, more cells survived outside spot irradiation, which is due to single chemotherapy effect of Au NRs@DSFDSs NPs. These proved that Au NRs@DSFDSs NPs had excellent PTT, which could kill the MCF-7 cells with CT synergistically.

The *in vitro* antitumor efficacy of Au NRs@DSFDSs NPs against MCF-7 cells was evaluated by cell viability assay by the Cell Counting Kit-8. Taking PBS-treated MCF-7 cells as control, the activity of MCF-7 cells, treated by free DOX, Au NRs +1300 nm laser, Au NRs@DSFDSs NPs and Au NRs@DSFDSs NPs+1300 nm laser, decreased significantly with the increase of nanoparticles concentration and indication time (Fig. S15b, c and S16). After treatment with free DOX, Au NRs+1300 nm laser, Au NRs@DSFDSs NPs and Au NRs@DSFDSs NPs +1300 nm laser for 24h, the cell viability of MCF-7 cells were 35%, 48%, 42% and 19%, respectively. Combination index (CI) is usually used to assess the synergistic effect of different agents or therapies. A CI value of 1 is indicative of an additive action, while a CI value of less than 1 indicates synergy. The CI value can be calculated by the following equation:  $CI = [IC_{50}(\text{combination CT})/IC_{50}(\text{CT})] + [IC_{50}(\text{combination PTT})/IC_{50}(\text{PTT})]$ . As shown in Figure 8a, the free DOX and Au NRs@DSFDSs NPs had an  $IC_{50}$  of  $0.92 \mu\text{g}\cdot\text{ml}^{-1}$  and  $1.70 \mu\text{g}\cdot\text{ml}^{-1}$  based on single chemotherapy for MCF-7 cells. Based on single PTT, the  $IC_{50}$

of Au NRs is  $0.68 \mu\text{g}\cdot\text{ml}^{-1}$ . For CPTT, Au NRs@DSFDSs NPs has an  $\text{IC}_{50}$  of  $0.13 \mu\text{g}\cdot\text{ml}^{-1}$  for PTT and  $0.31 \mu\text{g}\cdot\text{ml}^{-1}$  for CT. A CI value of 0.53 was obtained for CPTT, indicating a good synergistic therapeutic effect.<sup>[5-7]</sup>

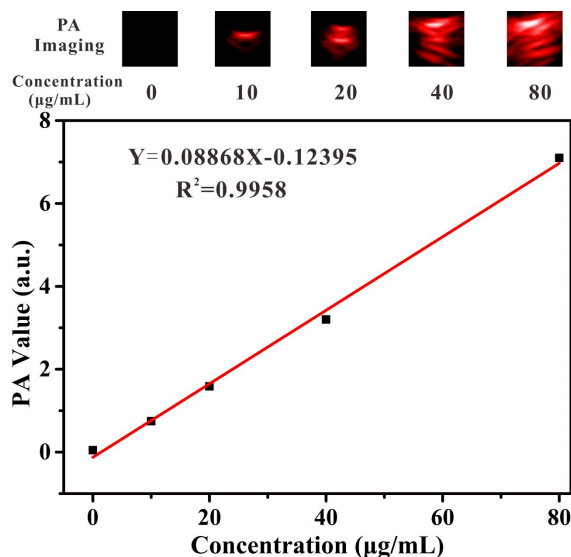


**Fig. S17** PA performance of Au NRs@DSFDS NPs. PA images and corresponding intensity of Au NRs @DSFDS NPs at various concentrations.

The real-time small-animal fluorescence imaging was used to observe the biodistribution and metabolism of Au NRs@DSFDSs NPs in nude mice (shown in Fig. 3a). The nude mice bearing a MCF-7 solid tumor were injected with PBS, free DOX, DOX-CysM-CPPZ NPs or Au NRs@DSFDSs NPs. For free DOX-treated nude mice, the DOX signal peaked in the whole body at 1h and then decreased quickly. There is little red in the whole body after 24 h, which was ascribed to metabolic elimination of free DOX via urine. However, the red fluorescence signal of nude mice treated with DOX-CysM-CPPZ NPs or Au NRs@DSFDSs NPs gradually increased at the beginning 6 h, and an intense signal remained in the tumor after 24h, indicating good passive targeting and accumulation on the tumor. The longer the retention time is, the higher the accumulation mass of Au NRs@DSFDSs NPs within tumor sites is.

In addition, the accumulation mass of DOX in the main organs and tumors was measured. As shown in Fig. 3b and 3c, for free DOX, accumulation mass of DOX in liver is really high and hardly any was found in the tumor. In contrast, a higher accumulation mass of DOX was found in tumor of nude mice treated by Au NRs@DSFDSs NPs or DOX-CysM-CPPZ NPs. Mean fluorescence intensity (MFI) value showed that accumulation mass of DOX in tumor tissue is even higher than other organs (Fig. 5c). These results proved that Au NRs@DSFDSs NPs could accumulate within the tumor via the EPR effect, which can successfully localize the tumor and monitor the process of cancer treatment.

Due to the excellent photothermal property, Au NRs can serve as the contrast agent for PA imaging under 1300 nm laser excitation. The PA signal intensities of Au

NR@DSFDSs NPs with different concentrations in PBS, indicating that the linear regression relation between PA intensity and the concentration of Au NR@DSFDSs NPs (Fig. S17). After injection into MCF-7 tumor-bearing mice with Au NR@DSFDSs NPs solution (38.4 mg Au/kg body weight), the PA imaging at 1300 nm wavelength was performed and recorded at set time points (0, 2, 6, 12, and 24 h ). With time going in the beginning, the PA signal intensity has a significant enhancement in the tumor region (Fig. 3d). Then, the PA signal intensity reached a maximum at 24 h. This result also indicates the accumulation of Au NR@DSFDSs NPs at the tumor site by EPR effect, which is beneficial for cancer treatment. The PA signal intensities of the tumor region in mice treated with Au NR@DSFDSs NPs are stronger than that of the tumor region in mice treated with Au-CysM NRs, indicating that Au NR@DSFDSs NPs could more easily accumulate at the site of the tumor due to the DOX-CysM-CPPZ surface coating.

To explore the photothermal effect of AuNR@DSFDSs NPs in tumor-bearing mice, the mice were irradiated with 1300 nm laser ( $1.5 \text{ W}\cdot\text{cm}^{-2}$ ) for 5 min and simultaneously the PT imaging of whole-body was obtained after the AuNR@DSFDSs NPs (38.4 mg Au/kg body weight) or PBS was injected into the mice by the tail vein for 24 h. With the irradiation time going, compared with the negligible temperature increase of the mice treated with PBS, the local tumor region temperature of the mice treated with AuNR@DSFDSs NPs increased and reached  $53.6^\circ\text{C}$  finally (Fig. 3d, e), indicating the efficient ablation of the tumor.

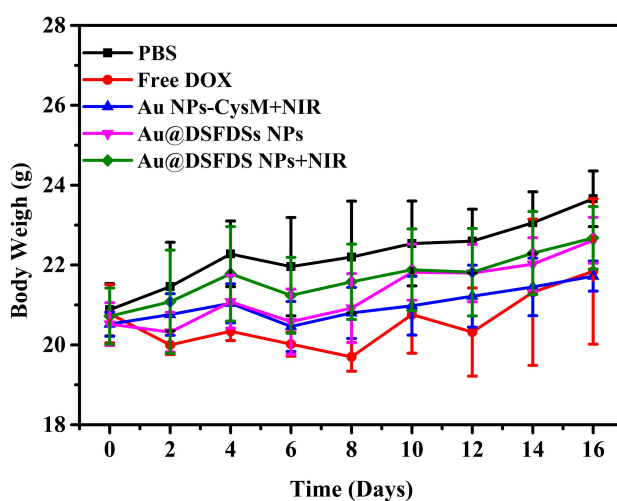


**Fig. S18** Relative mice body weights during the whole treatment period.

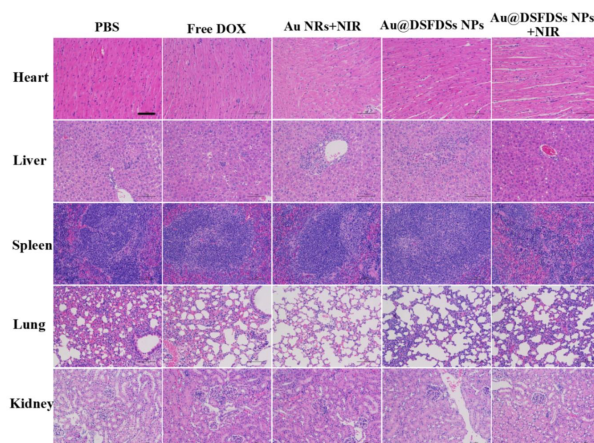


**Fig. S19** H&E staining for the key organs. Scale bar is 100  $\mu\text{m}$ .

The treatment effect of Au NRs@DSFDSs NPs against MCF-7 tumor-bearing mice was investigated. When the tumor volume was about 100  $\text{mm}^3$ , the tumor-bearing mice were stochastically divided into 5 groups (five mice per group) and treated with (1) PBS, (2) free DOX, (3) AuNR + NIR-II laser, (4) Au NRs@DSFDSs NPs, or (5) Au NRs@DSFDSs NPs + NIR-II laser respectively. During the treatment course, the injection was performed six times (Fig. 4a). The treatment effect was estimated by the relative tumor volumes of each group recorded every other day. Previous reports had confirmed that only laser irradiation or Au NRs alone had a negligible effect on tumor inhibition. The group treated with PBS, free DOX, AuNR + NIR-II laser, Au NRs@DSFDSs NPs or Au NRs@DSFDSs NPs + NIR-II laser respectively displayed 13.7-, 12.5-, 5.3-, 2.28--fold increases or 99% decrease of tumor volume at the end of the 16 days therapy course (shown in Fig. 4a and 4c). The free DOX group exhibited a moderate therapeutic efficacy, which may be due to the poor enrichment of tumor site (Fig. 4a). However, the other three therapy groups exhibited much better efficacy of tumor inhibition during the treatment course. Remarkably, the combined therapy group (Au NRs@DSFDSs NPs + NIR-II laser) exhibited the lowest relative tumor volume and the best efficacy of tumor inhibition. At the end of the 16 days therapy course, the mice were sacrificed humanely, and the images for the representative tumors of each group are exhibited (Fig. 4b). After the treatment course, the tumor weights and tumor inhibition ratios (TIRs) of every group were also obtained (Fig. 4c). Compared with other therapy group, the combined CPTT group (Au NRs@DSFDSs NPs + NIR-II laser) displayed the lowest tumor weight and highest TIR, indicating the better treatment efficacy. Meanwhile, the record of the body weights of each treatment groups were kept during the whole treatment, and mean values were calculated and displayed (Figure S18). During the therapy course, the body weight of each group have increased mildly, indicating that the systemic toxicity of the injection with Au NRs@DSFDSs NPs + NIR-II laser were negligible. After the course of treatment, hematoxylin/eosin (H&E) staining were finished for the histological examinations of tumor tissue sections. Comparison with the PBS groups, the tumor cell of the other groups became fewer and displayed typical features of apoptotic cells involving cell shrinkage and loss of contact (Fig. 4d). In particular, the

combined CPTT group (Au NRs@DSFDSs NPs + NIR-II laser) exhibited the highest apoptosis level and the fewest cancer cells. To sum up, these experiment data indicated that the TME stimuli-responsive DSFDSs polymer coating and Au NR could afford a good combined action of chemotherapy and PTT to achieve high antitumor efficacy *in vivo*.

At the end of the 16 days therapy course, to evaluate the biosafety of the Au NRs@DSFDSs NPs, the major organs (heart, liver, spleen, kidney, and lung) were harvested after the mice of different treatment group were sacrificed. The H&E staining images of tissue sections for major organs were obtained (Fig. S19), and no obvious organ abnormality or inflammation lesion was observed, indicating high biosafety of Au NRs@DSFDSs NPs *in vivo*.

## REFERENCES

1. X. Ye, C. Zheng, J. Chen, Y. Gao and C. B. Murray, *Nano Lett.* **2013**, *13*, 765–771.
2. S.L. Hou, S.S. Chen, Z. Huang and Q. Lu, *J. Mater. Chem. B* **2019**, *7*, 4319–4327.
3. M. Almada, B.H. Leal-Martínez, N. Hassan, M.J. Kogan, M.G. Burboa, A. Topete, M.A. Valdez and J. Juárez, *Mate. Sci. Eng. C* **2017**, *77*, 583–593.
4. Q. Tian, F. Jiang, R. Zou, Q. Liu, Z. Chen, M. Zhu, S. Yang, J. Wang, J. Wang and J. Hu, *ACS Nano* **2011**, *5*, 9761–9771.
5. X. Wu, L. Zhou, Y. Su and C.M. Dong, *Biomacromolecules* **2016**, *17*, 2489–2501.
6. Ma, L.; Kohli, M.; Smith, *ACS Nano*. **2013**, *7*, 9518–9525.
7. S. Mignani, M. Bryszewska, B. Klajnert-Maculewicz, M. Zablocka and J. P. Majoral, *Biomacromolecules* **2015**, *16*,1-27.